Global Distribution of Hot Towers in Tropical Cyclones Based on 11-Yr TRMM Data

CHENG TAO AND HAIYAN JIANG

Department of Earth and Environment, Florida International University, Miami, Florida

ABSTRACT

Global distribution of hot towers in tropical cyclones (TCs) is statistically quantified using an 11-yr Tropical Rainfall Measuring Mission (TRMM) Tropical Cyclone Precipitation Feature (TCPF) database. From 6003 individual TRMM overpasses of 869 TCs, about 1.6% of TC convective systems are found to penetrate 14 km and about 0.1% of them even reach the 380-K potential temperature level. Among six TC-prone basins, the highest population of TC convective systems and those with hot towers are found over the northwest Pacific (NWP) basin. However, the greatest percentage of TCPFs that are hot towers [overshooting TCPFs (OTCPFs)] is found over the North Indian Ocean basin. Larger overshooting distance and ice mass are also found in this basin. The monthly variation of OTCPFs resembles that of TC activities in each basin. The percentage of OTCPFs is much higher in the inner core (IC) region (10%) than that in the inner rainband (IB; 2%) and outer rainband (OB; 1%) regions. OTCPFs in the IC region have much larger overshooting distance, area, volume, and ice mass than those in the IB and OB regions. The percentage of OTCPFs in the IC region increases as both TC intensity and intensification rate increase. About 17% of IC features in rapidly intensifying storms penetrate over 14 km, while the percentage is down to 11% for slowly intensifying, 9% for neutral, and 8% for weakening storms. A very good linear relationship is found between TC intensification rate and the percentage of TCPFs that are hot towers in the IC region.

1. Introduction

Hot towers are horizontally small, deep tropical cumulonimbus clouds with intense rapidly rising cores that reach or penetrate the tropopause. Several decades of studies have shown that they play a crucial role on the maintenance of global circulation (Yulaeva et al. 1994; Rosenlof 1995). They are also an essential agent for heat and moisture transportation (Riehl and Malkus 1958; Simpson 1990) as well as mass exchange between tropopause and stratosphere (Holton et al. 1995; Dessler 2002). In the past decades, radar, passive microwave, and infrared (IR) observations have been used to investigate the geophysical, seasonal, and diurnal distribution of deep convection in the tropics (Hall and Vonder Haar 1999; Petersen and Rutledge 2001; Gettelman et al. 2002; Jiang et al. 2004; Liu and Zipser 2005, hereafter LZ05). Based on IR and visible satellite data, deep convective clouds were identified using a −65°C cloud-top brightness temperature threshold, and the diurnal cycle of west Pacific deep convection was examined by Hall and Vonder Haar (1999), who noted that "the diurnal cycle of deep convective cloud is driven by the internal variation of large clusters." Based on IR brightness temperatures from satellites and contemporaneous reanalysis temperatures, Gettelman et al. (2002) found out that convection penetrating the tropopause is most common in Northern Hemisphere winter globally, while regionally the strongest and deepest convection is found over the central and western Pacific in February and over the Indian monsoon in August. Also, a relationship between cold tropopause temperatures and deep convection is discovered: convection penetrates most frequently at the places where the tropopause is coldest. LZ05 studied the common properties of global deep convection penetrating the tropical tropopause and noted that overshooting convection is much more frequent over land than over ocean, and the most intense deep tropical convection was detected over central Africa using a 5-yr Tropical Rainfall Measurement Mission (TRMM) database.

However, existing studies mostly focused on deep convection in general convective systems. Since there

---

Corresponding author address: Dr. Haiyan Jiang, Department of Earth and Environment, Florida International University, 11200 SW 8th Street, PC-342B, Miami, FL 33199.
E-mail: haiyan.jiang@fiu.edu

are moist ascents regions within tropical cyclones (TCs), an interesting question in TC research is whether these deep convective systems in TCs are subject to a different amount of entrainment drying compared with other mesoscale systems. Romps and Kuang (2009) examined deep convection penetrating the tropopause in TCs using 23 years of satellite IR, best-track, and reanalysis data. In their study, an overshooting cloud is identified when its infrared brightness temperature is below the monthly averaged tropopause temperature. They suggested a disproportionate percentage of global overshooting cloud tops occurred in TCs.

On the other hand, some previous studies suggested that hot towers occurring within the inner core region are related to the intensification of TCs (Hendricks et al. 2004; Kelley et al. 2004, 2005; Montgomery et al. 2006; Houze et al. 2009; Jiang 2012). Kelley et al. (2004), using 6 years of the well-centered overflights of TCs observed by the TRMM precipitation radar (PR), argued that the chance of TC intensification increases when one or more tall precipitation cells exist in the eyewall. An extremely tall convective tower in their study is identified when the 20-dBZ reflectivity signal reaches or penetrates 14.5 km. Hendricks et al. (2004) analyzed a high-resolution near-cloud-resolving numerical simulation of Hurricane Diana (1984). They demonstrated that the cores of deep cumulonimbus convection possessing strong vertical vorticity (they called these "vortical hot towers") are the preferred mode of convection and they are of great importance in the formation of the tropical storms via a two-stage process. Montgomery et al. (2006), using a nonhydrostatic cloud mode, examined the role of vortical hot towers in the process of transforming a midtropospheric cyclonic vortex into a warm core tropical depression. They proposed that these intense vortical hot towers may initiate TC genesis. Using 11 years of TRMM data, Jiang (2012) examined the hypothesis of hot towers in the inner core as an indicator of RI. In her study, hot towers are defined when the 20-dBZ radar echo height is at or above 14.5 km. She found that for samples with hot towers in the inner core, the probabilities of rapid intensification (RI) and slow intensification (SI) increase, but hot towers are neither a necessary nor a sufficient condition for RI.

With the first-ever satellite-based precipitation radar, TRMM is not only invaluable for global precipitation estimates (Adler et al. 2000; Schumacher and Houze 2003); it also can be used to quantify the properties of cloud systems and their distributions throughout the global tropics (Nesbitt et al. 2000; Cecil et al. 2002, 2005). In this study, the global distribution of hot towers in TCs is quantified using 11-yr TRMM data. There are two main goals of this study. The first goal is to examine how hot towers in TCs are distributed geographically and seasonally and to determine the fraction of hot towers out of total TC convective systems. The second goal is to find out the distribution of hot towers in different TC regions, intensities, and intensity change stages. In addition, the overshooting distance, area, volume, mass, and convective proxies of hot towers in TCs are examined. The key questions to be addressed are the following: 1) What are the geographical distribution of population and overshooting properties of hot towers in TCs? Is the overshooting activity more frequent and intense over the northwest Pacific basin? 2) What are the patterns of seasonal variation of population and overshooting properties of hot towers in TCs? 3) How are hot towers distributed in different TC regions? Is overshooting convection most intense in the inner core region? 4) Are hot towers within the inner core region related to TC intensity and intensity change? In section 2, the data and methodology applied to identify hot towers in TCs and selected overshooting properties used in this study are described. The main results are presented in section 3, and conclusions are given in section 4.

2. Data and methodology

a. TRMM TCPF database

The data for this study include 11-yr (January 1998–December 2000 and January 2002–December 2009) observations by TRMM. In August 2001, the altitude of TRMM satellite was boosted from 350 to 402 km to lengthen its lifetime in orbit. Considering that the quality of radar data is questionable during the orbit boost, we exclude the data from year 2001. Grouping continuous pixels satisfying certain criteria into precipitation features (PFs), a University of Utah (UU) TRMM database has been built (Nesbitt et al. 2000; Liu et al. 2008) and successfully applied to many global and regional climatological studies (Cecil et al. 2002, 2005; Zipser et al. 2006). Currently, three levels of processing of the TRMM data are constructed in the database, including various TRMM observed properties such as feature size, mean rain rate, maximum 20-dBZ height, etc. The environmental sounding for each PF are obtained by interpolation from 2.5° × 2.5°, 6-h interval National Centers for Environmental Prediction (NCEP) reanalysis data described by Kistler et al. (2001).

To focus on TCs specifically, a TC subset of the UU TRMM PF database based on the collaboration between Florida International University (FIU) and UU has been generated (Jiang et al. 2011). This FIU–UU TRMM TC precipitation, cloud, and convective cell

TABLE 1. Population, overshooting distance, and area of OTCPFs identified with respect to five different reference heights.

Reference heights	14 km	LNB$_{sfc}$	LNB$_{925\&1000}$	Z_{trop}	Z_{380K}
OTCPFs population	2368	1185	464	295	137
Number of orbits	1690	939	388	277	130
Number of TCs	686	493	268	227	119
Population percentage (%)	1.59	0.79	0.31	0.20	0.09
Mean reference height (km)	14.00	14.73	14.45	16.39	16.91
Mean Z_{20dBZ} (km)	15.29	15.88	15.80	17.20	17.91
Mean overshooting distance (km)	1.29	1.16	1.34	0.81	1.00
Mean OTCPFs overshooting area (km^2)	278	287	297	225	221
Mean overshooting area/OTCPF raining area (%)	7.45	9.53	7.65	5.40	8.47
Total overshooting area/total raining area (%)	0.32	0.17	0.07	0.03	0.01

feature (TCPF) database is built by interpolating the global TC best-track data into the UU TRMM PF database. A TCPF is identified when the distance between TC center and the TRMM PF center is within 500 km. Besides existing TRMM observed properties in the UU TRMM PF database, a series of storm-related parameters are calculated and linearly interpolated into TRMM observation time—for example, land–ocean flags of TC center, storm 12-, 24-, 36-, and 48-h future intensity changes, etc. Furthermore, based on this FIU-UU TRMM TCPF database, three subregions—the inner core (IC), inner rainband (IB), and outer rainband (OB)—are subjectively sorted for each individual TRMM TC overpass (Jiang et al. 2013).

This study uses the TRMM TCPF database to identify TC convective systems. The comprehensive database contains 13 precipitation feature definitions based on different grouping criteria [see Jiang et al. (2011) for details]. In this study, each TCPF is grouped by contiguous pixels with TRMM PR 2A25 (Iguchi et al. 2000) near-surface rain rate greater than zero. To minimize noise, the minimum near-surface four adjacent pixels with rain rate greater than zero (about 80 km^2) were required for every TCPF. Here, we only consider TCPFs over ocean. As a result, more than 150 000 TCPFs were found within the 11-yr period from 6003 individual TRMM overpasses of 869 TCs. The TRMM observation is between 36°S and 36°N. Six TC-prone basins are considered in this study following Jiang and Zipser (2010): Atlantic (ATL), east central Pacific (EPA), northwest Pacific (NWP), North Indian Ocean (NIO), South Indian Ocean (SIO), and South Pacific (SPA).

b. Methodology of defining hot towers in TCPFs and selection of overshooting properties

Five reference heights are selected to identify TCPFs with overshooting tops (OTCPFs; i.e., hot towers), following the criteria of LZ05. These include 1) 14 km, 2) level of NCEP reanalysis tropopause (Z_{trop}), 3) level of potential temperature θ equal to 380 K (Z_{380K}) calculated from NCEP sounding, 4) level of neutral buoyancy (LNB) calculated using NCEP soundings and surface equivalent potential temperature θ_e (LNB$_{sfc}$), and 5) level of neutral buoyancy calculated using θ_e at 925 and 1000 mb, whichever is greater (LNB$_{925\&1000}$). Then OTCPFs are found from 150 000 TCPFs when the maximum 20-dBZ echo height observed by TRMM PR exceeds above-mentioned reference heights respectively. Therefore, one TCPF represents one precipitating system in TCs and one OTCPF represents one hot tower in TCs in this study. As pointed out by LZ05, OTCPFs defined here are representing the area of large ice particles lifted above the reference heights by strong updrafts in convective cores. Unlike using the IR and cloud radar data, anvils clouds with small ice particles are not detectable by the PR and are not included in this study.

To describe overshooting properties of hot towers in TCs, four overshooting parameters (i.e., overshooting distance, area, volume, and precipitating ice mass) are selected and calculated for each OTCPF using the same method as LZ05. The overshooting distance for each OTCPF refers to the distance between the maximum height of 20 dBZ and the reference height. The overshooting area of each OTCPF is calculated by multiplying the total number of pixels with PR reflectivity greater than 20 dBZ by the size of each pixel at the reference level. Similarly, the overshooting volume and ice mass for each OTCPF are calculated by integrating the volume and precipitating ice mass of overshooting pixels above the reference height. Table 1 displays the characteristics, such as population, mean overshooting distance, and overshooting area of the identified OTCPFs based on five different reference heights. The mean reference heights in TCs over oceanic regions
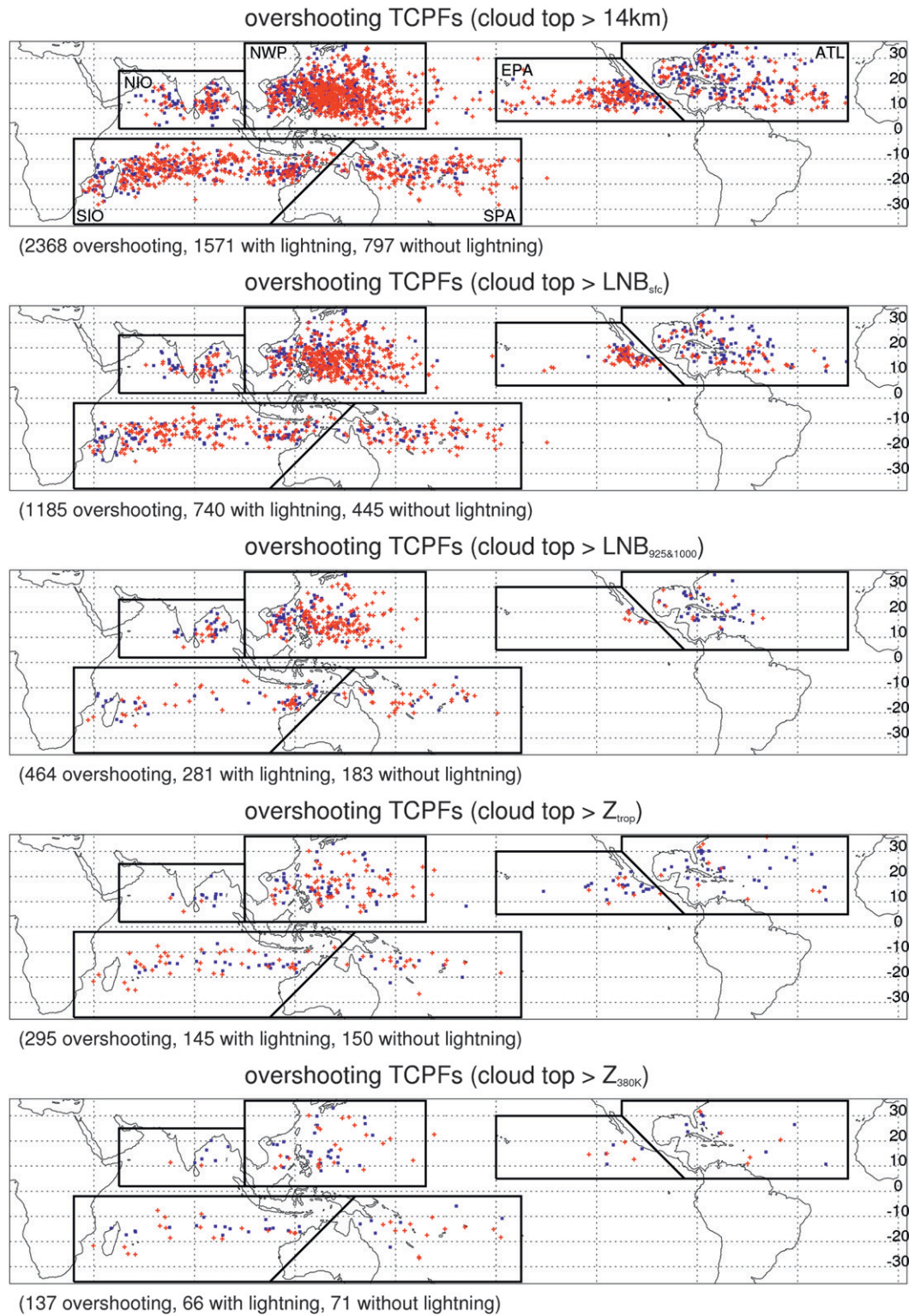
overshooting TCPFs (cloud top > 14km)

(2368 overshooting, 1571 with lightning, 797 without lightning)

overshooting TCPFs (cloud top > LNB$_{sfc}$)

(1185 overshooting, 740 with lightning, 445 without lightning)

overshooting TCPFs (cloud top > LNB$_{925\&1000}$)

(464 overshooting, 281 with lightning, 183 without lightning)

overshooting TCPFs (cloud top > Z$_{trop}$)

(295 overshooting, 145 with lightning, 150 without lightning)

overshooting TCPFs (cloud top > Z$_{380K}$)

(137 overshooting, 66 with lightning, 71 without lightning)

FIG. 1. Location of identified OTCPFs at 36°N–36°S using different reference heights. The OTCPFs with lightning are shown in red, and the OTCPFs without lightning are shown in blue.
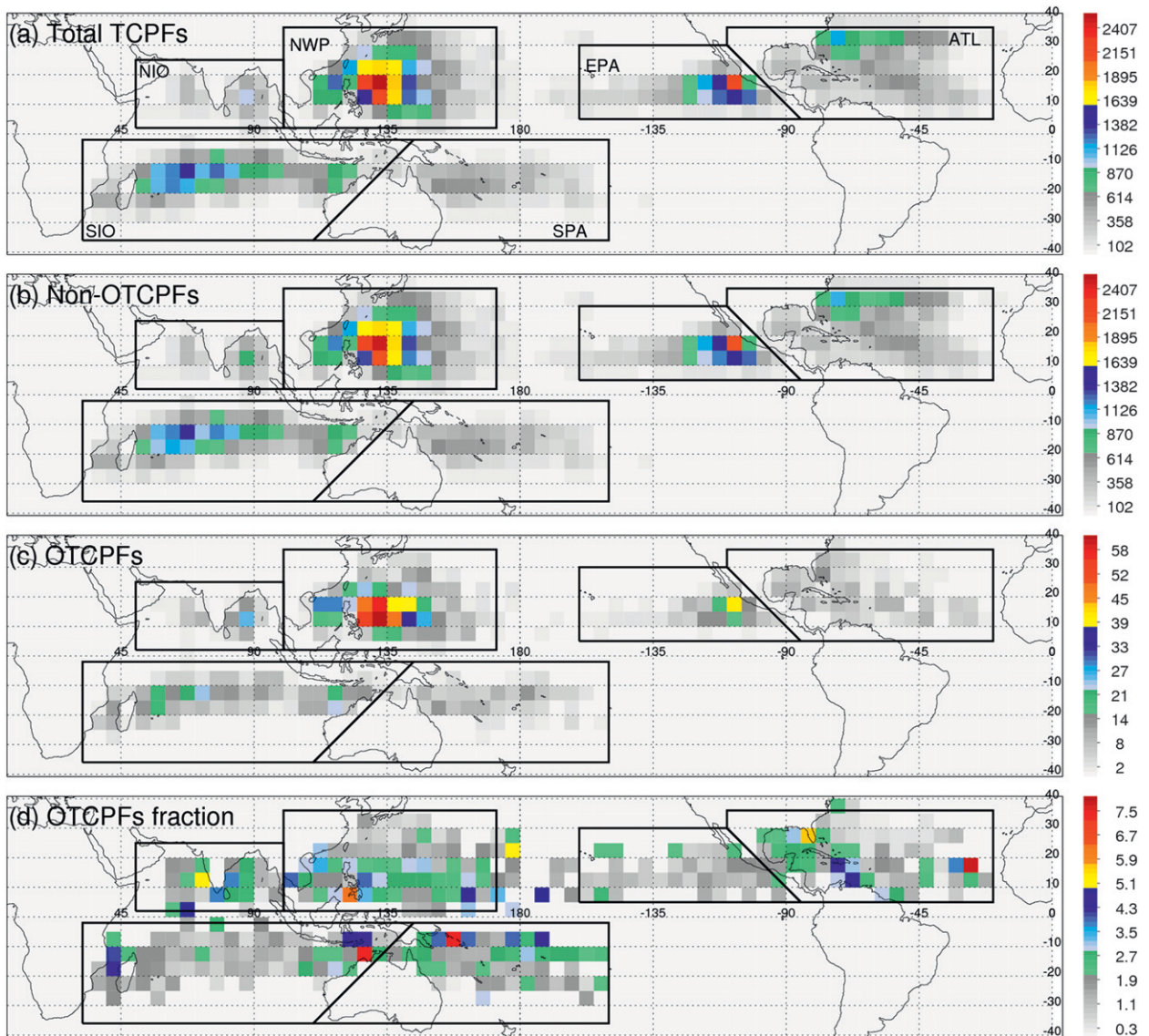
FIG. 2. Global distribution of (a) population of total TCPFs, (b) population of TCPFs without hot towers, (c) population of OTCPFs, and (d) OTCPFs fraction (%) based on a $5° \times 5°$ grid for the years of 1998–2000 and 2002–09. Borders of six basins (ATL, EPA, NWP, NIO, SIO, and SPA) are indicated.

between 36°S and 36°N as shown in Table 1 are similar to those for general tropical regions between 20°S and 20°N presented in LZ05. Of the five definitions for OTCPF, the mean Z_{380k} is the highest at 16.9 km. From a total of 150 313 TCPFs, 1.59% of them have 20-dBZ radar echoes at or above 14 km, while only 0.09% of TCPFs are found reaching the level of potential temperature equal to 380 K. Compared with LZ05's result of 1.38% overshooting PFs for the 14-km reference height, the percentage of OTCPFs is slightly higher. The mean overshooting distance of OTCPFs for the 14-km reference height is 1.29 km, slightly lower than that for general overshooting PFs presented in LZ05. However,

the mean overshooting distance of OTCPFs for the Z_{380k} reference height is 1 km, which is about 0.4 km higher than that derived in LZ05. On average, about 7.5% of OTCPF raining area detected by the PR has overshooting above 14 km from these OTCPFs. LZ05 found that when higher reference heights were used, the PFs tend to have a larger overshooting area and smaller raining area. This is not the case for TCPFs. The difference is due to isolated severe convective storms over land included in LZ05's dataset.

Figure 1 demonstrates the locations of OTCPFs for different reference heights. The pattern of geographical distribution of OTCPFs shows little sensitivity to

TABLE 2. Population of TCPFs, TCPFs without hot towers, OTCPFs, and fraction of OTCPFs in different TC basins.

Basin	ATL	EPA	NWP	NIO	SIO	SPA	Total
TCPFs	26 697	20 751	49 019	6040	34 681	13 125	150 313
Non-OTCPFs	26 394	20 501	48 060	5913	34 170	12 907	147 945
OTCPFs	303	250	959	127	511	218	2368
OTCPFs	1.13	1.20	1.96	2.10	1.47	1.66	1.58

different reference heights. This is also the case when examining overshooting properties. Also shown in Fig. 1 are the lightning properties of the OTCPFs, where the red represents the OTCPFs with lightning and blue indicates the OTCPFs without lightning. When higher reference heights are used, fewer OTCPFs with lightning are detected. It is found that over 66% of OTCPFs have lightning when using 14 km as a reference level. And this percentage decreases to 48% for TCPFs reaching the level of 380-K potential temperature. Considering the smaller numbers of OTCPFs when using higher reference heights, in this study the 14-km reference height is applied to examine the global and seasonal distributions of OTCPFs in different TC regions, intensities, and intensity change stages. Therefore, in total, 2368 OTCPFs from 1690 TRMM overpasses of 686 TCs are included in the rest of the study.

3. Results

a. Geographical and seasonal distribution of population and overshooting properties of OTCPFs

1) GEOGRAPHICAL DISTRIBUTION

The geographical distributions of populations of total TCPFs, TCPFs without hot towers, OTCPFs, and the fraction of TCPFs that are hot towers are presented in Fig. 2. To create this plot, populations of TCPFs, TCPFs without hot towers, OTCPFs, and the fraction of OTCPFs are summed into $5° \times 5°$ longitude–latitude grid boxes. The general distribution pattern and locations of highest number concentration of total TCPFs (Fig. 2a) and TCPFs without hot towers (Fig. 2b) are very similar, indicating that majority of total TCPFs do not penetrate the 14-km height. Precipitation and convective systems in TCs have the highest number population in the NWP basin over a large area east of the Philippine islands, followed by a smaller area in the EPA south of Baja California. Moderate number concentrations of TCPFs are seen in the SIO basin between 10° and 20°S east of Madagascar and the northwest coast of Australia and in the ATL basin near the east coast of the United States between 20° and 30°N. The overall

pattern is very similar to the patterns of global TC number density, accumulated cyclone energy (ACE), and precipitation presented in Jiang and Zipser (2010).

The geographical distribution of population of OTCPFs (Fig. 2c) is similar to that of total TCPFs (Fig. 2a) and TCPFs without hot towers (Fig. 2b). The highest concentration of OTCPFs is over NWP and EPA around the same locations as in total TCPFs. Moderate number concentrations of OTCPFs are also seen in the SIO basin between 10° and 20°S east of Madagascar and the northwest coast of Australia. But unlike total TCPFs, the population of OTCPFs across the whole ATL basin is relatively low. Consistent with the results here, previous studies have shown that the deepest and strongest oceanic tropical convection (Gettelman et al. 2002; LZ05) and TC convection (Jiang et al. 2011) are most common over NWP according to IR, radar, and 85-GHz passive microwave measurements. Several previous studies from the perspective of large-scale environmental factors also indicate that NWP has higher SST, lower wind shear (Gray 1968), and higher convective available potential energy (CAPE) and LNB (Liu et al. 2007) and therefore is more favorable for development of both TC and deep convection.

It is reasonable that OTCPFs concentrate over the places where precipitation and convective systems in TCs occur most frequently. The fraction of TCPFs that are hot towers is calculated for each $5° \times 5°$ grid box, and its distribution is shown in Fig. 2d. This plot gives us information about where TCPFs have higher opportunity to penetrate over 14 km. The pattern shown in Fig. 2d is very different from the distribution of population of TCPFs and OTCPFs seen in Figs. 2a–c. Higher fractions seem randomly scattered over the map, although there are several high values near the coastal regions.

Table 2 shows the population of TCPFs, TCPFs without hot towers, and OTCPFs, as well as the overall percentage of TCPFs that are hot towers in six TC basins. After dividing the total number of OTCPFs by the population of TCPFs in each basin, it is found that hot towers contribute, respectively, 2.10%, 1.96%, 1.66%, 1.47%, 1.20%, and 1.13% of TCPFs in NIO, NWP, SPA, SIO, EPA, and ATL. NIO has the highest percentage of OTCPFs, although populations of both total TCPFs and OTCPFs are low in this basin. NWP has the second highest percentage,
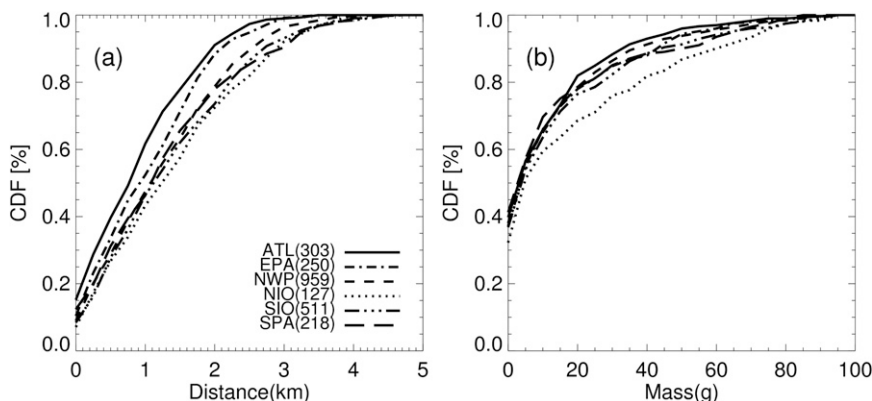
FIG. 3. Cumulative density functions (CDFs) of (a) overshooting distance, and (b) overshooting precipitating ice mass for the ATL, EPA, NWP, NIO, SIO, and SPA OTCPFs.

just slightly lower than that in NIO. Also, the height of tropopause in the NIO basin is the lowest among six TC-prone basins with a mean value of 13.4 km, indicating that the highest percentage of OTCPFs found in the NIO basin is not because of a higher tropopause.

The cumulative distribution functions (CDFs) of over-shooting distance and ice mass for each TC-prone basin are presented in Fig. 3. From Fig. 3a, it can be seen that OTCPFs over the NIO basin have the greatest over-shooting distance, followed by the SIO, NWP, SPA, EPA, and ATL basins. The difference of the median over-shooting distances between OTCPFs in the NIO and ATL basins is about 0.5 km. The distributions separate into roughly two groups, with higher overshooting distances in NIO, SIO, NWP, and SPA and smaller distances in ATL and EPA. As for the overshooting ice mass (Fig. 3b), it can be seen clearly that these properties are the highest for OTCPFs in the NIO basin, while the differences among other five TC basins are small. Note that unlike overshooting distance, the overshooting ice mass not only depends on the overshooting convection itself but is also related to the size of the extremely deep con-vective systems. Significance tests[1] have been done to determine the significant levels of the mean values for each overshooting parameter in six TC basins. It is shown that statistically significant differences exist among dif-ferent TC basins for overshooting distance at the 99% level and for overshooting ice mass at the 95% level. For overshooting area and volume, none of the differences among various TC basins is significant (not shown).

From Figs. 2 and 3, it is obvious that the NIO basin has the greatest percentage of TCPFs that are hot towers and the greatest overshooting properties although the NIO basin has the least population of OTCPFs. This may because that the NIO basin has a much smaller amount of small features with low maximum 20-dBZ echo height relative to other oceanic basins, as pointed out by Jiang et al. (2011).

2) SEASONAL DISTRIBUTION

To study the seasonal variations of the population of hot towers in TCs, monthly populations of TCs, TCPFs, and OTCPFs are first calculated for each basin. After dividing each monthly population by the corresponding total population, percentage monthly populations of TCs, TCPFs, and OTCPFs over six oceanic basins are presented in Figs. 4a–f. For each basin, the monthly percentages for TCs, TCPFs, and OTCPFs sum up to 100%, respectively. There is a strong seasonal variation of OTCPFs in each basin, which is similar to the seasonal variation of TC and TCPF populations. Two exceptions exist, one in NIO and one in SPA, where the monthly variation of OTCPFs shows significant difference from that of TCPFs and TCs. However, significant tests using analysis of variance statistical technique show that these differences among monthly fractions of OTCPFs, TCPFs, and TCs in the NIO and SPA basins are not statistically significant. This indicates that in all TC basins, the seasonal variation of OTCPFs is driven by the seasonal variation of TCs and convective sys-tems in TCs.

The monthly variations of overshooting distance, area, volume, and ice mass for six TC basins are dis-played in Figs. 5a–f. Similar to Fig. 4, the values of overshooting properties for each OTCPF are added up together for each basin monthly and then divided by the corresponding total value in the same basin. For

---

[1] A one-way analysis of variance (function KW_TEST in In-teractive Data Language (IDL) version 8.0) has been applied to Figs. 3, 4, 5, 7, and 9 to test the hypothesis that three or more sample populations have the same mean of distribution against the hy-pothesis that they differ.
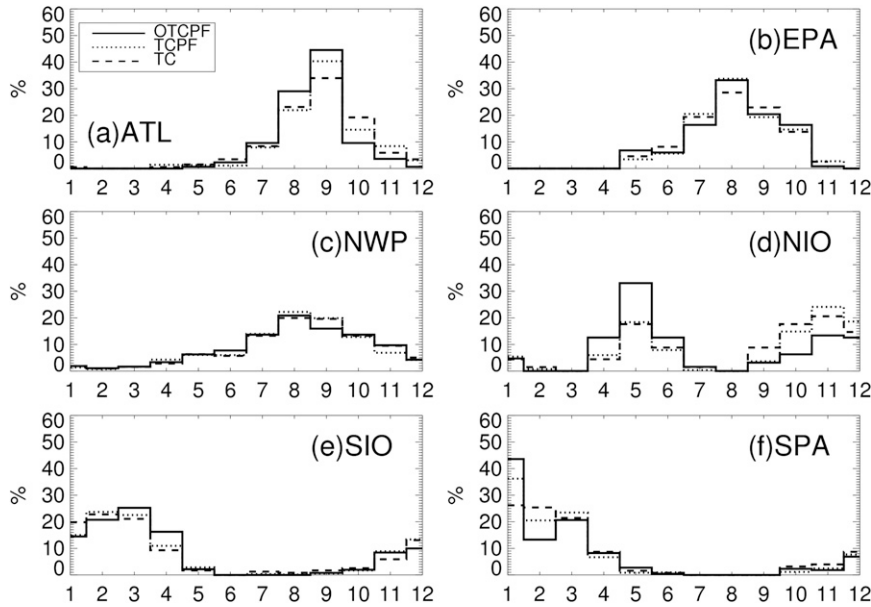
FIG. 4. Monthly variation of population of OTCPFs, TCPFs, and TCs in the (a) ATL, (b) EPA, (c) NWP, (d) NIO, (e) SIO, and (f) SPA basins.

example, to get the variation of overshooting distance for OTCPFs in the ATL basin, the values of overshooting distance of each ATL OTCPF are summed up together for each month, and then divided by the total overshooting distance for identified OTCPFs in the ATL basin. The monthly percentage for each overshooting property in Fig. 5 sums up to 100% for each

basin. The general patterns for different overshooting properties are similar to each other for each basin, and are similar to the monthly variation for the population of OTCPFs shown in Fig. 4. For the NIO basin, over 40%–55% of overshooting distance, volume, and mass concentrates in May. There are some small fluctuations in December in the NIO basin and in August, September,
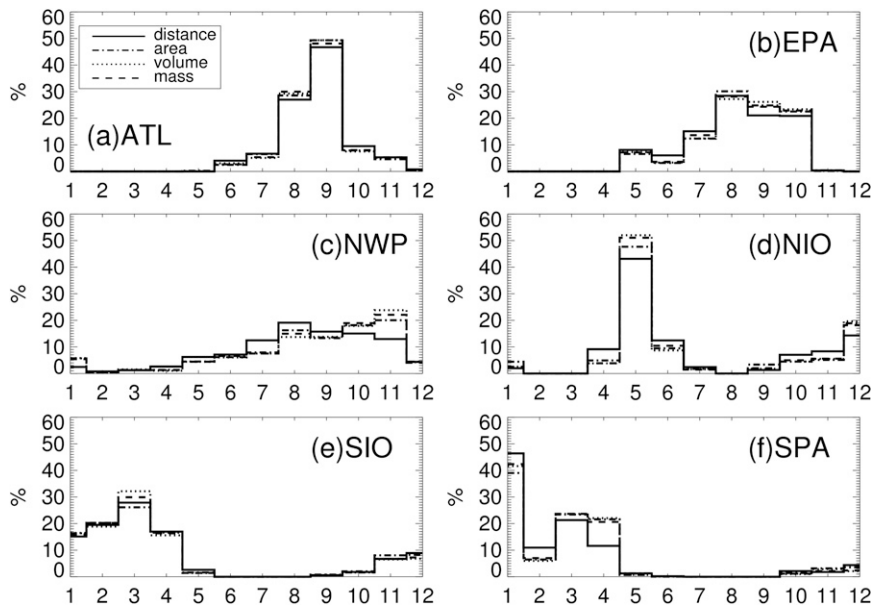

FIG. 5. Monthly variation of overshooting distance, area, volume and precipitating ice mass of OTCPFs in the (a) ATL, (b) EPA, (c) NWP, (d) NIO, (e) SIO, and (f) SPA basins.

TABLE 3. Mean radius of IC, IB, and OB regions, and populations of TCPFs and OTCPFs and the percentage of OTCPFs in the IC, IB, and OB regions.

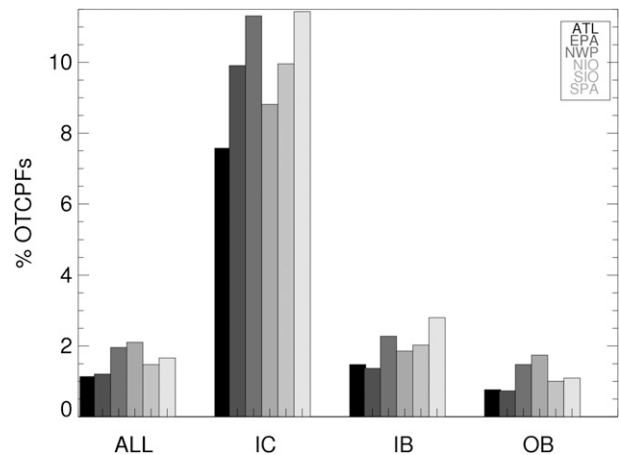| Region	Mean radius (km)	Population of OTCPFs	Population of TCPFs	Percentage of OTCPFs (%)
IC	82	615	6119	10.05
IB	162	337	17 568	1.92
OB	502	1416	126 626	1.19

FIG. 6. The percentage of OTCPFs for six TC-prone basins in all TC regions, in the inner core (IC), inner rainband (IB), and outer rainband (OB) regions only for from left to right the ATL, EPA, NWP, NIO, SIO and SPA basins.

and November in the NWP basin, which are different from the seasonal variation of the OTCPF population in Fig. 4c. However, significance tests using the analysis of variance show that these small peaks are not statistically significant. The overall result suggests that the monthly variation of overshooting properties is driven by monthly TC activities.

b. The distribution of population and overshooting properties of OTCPFs as a function of TC regions, TC intensities, and TC intensity change stages

1) TC REGIONS

Fixed radii have been used to study different TC regions in many previous studies. To account for varying TC sizes, a semi-manual separation of inner core, inner rainband, and outer rainband regions for all the TRMM TC overpasses during 1998–2009 has been accomplished by Jiang et al. (2013). This separation is based on the concept described by Cecil et al. (2002) using TRMM TMI and PR observations. Different from Cecil et al. (2002), TC overpasses with and without eyewalls are both included. The IC region includes complete eyewalls and all near-center convection for storms without eyewalls. The IB region includes banded or bloblike precipitation immediately outside of the IC boundary. The OB region includes outward spiraling banded precipitation and any TC-related precipitation features located about 150–200 km beyond the storm center.

Table 3 lists the mean radius, populations of TCPFs and OTCPFs, and the percentage of OTCPFs in the IC, IB, and OB regions for the 11-yr TRMM TCPF data used in this study. The mean extents of the IC, IB, and OB regions are 82, 162, and 502 km, respectively. There are 615, 337, and 1416 hot towers (OTCPFs) found in the IC, IB, and OB regions, respectively. It is not surprising that the OB region has most OTCPFs since it has the largest area. However, the percentage of OTCPFs in the OB region is the lowest. Whereas 10.05% of TCPFs in the IC region penetrate over 14 km, only 1.92% and 1.19% of TCPFs are OTCPFs in the IB and OB regions,

respectively. The percentage of TCPFs that are hot towers calculated for each TC basin in different TC regions is presented in Fig. 6. It can be seen that although in all TC regions the largest percentage of TCPFs reaching 14 km is found in the NIO basin, that is not the case for the IC and IB regions. In the IC region, TCPFs over the SPA and NWP basins have the highest chance to penetrate over 14 km with a percentage of OTCPFs of ~11%. A lower percentage of IC OTCPFs is found in the EPA and SIO basins (about 10%). The IC TCPFs in the ATL and NIO basins have the lowest percentages of hot towers (7.6% and 8.8%, respectively). In the IB region, the highest percentage of OTCPFs is found in SPA, followed by NWP, SIO, NIO, ATL, and EPA in the decreasing order. In the OB region, TCPFs in the NIO basin have the highest opportunity to penetrate over 14 km (1.74%), followed by NWP, SPA, SIO, ATL, and EPA. This indicates that the greatest percentage of hot towers found over NIO basin in all TC regions is mostly contributed by the OB region, which has the largest amount of TCPFs. A Pearson's chi-squared test[2] has been done for Fig. 6 and it shows that statistically significant differences exist among the percentages of TCPFs that are hot towers for various TC intensity stages in all TC regions and in the IC, IB, and OB regions only at the 95% level.

---

[2] A Pearson's chi-squared test for independence is to determine whether there is a significant association between two or more variables. In this study, it is used to determine whether there is a significant association between the percentages of TCPFs that are hot towers in different TC basins (Fig. 6), TC intensity stages (Fig. 8), and TC intensity change stages (Fig. 10).
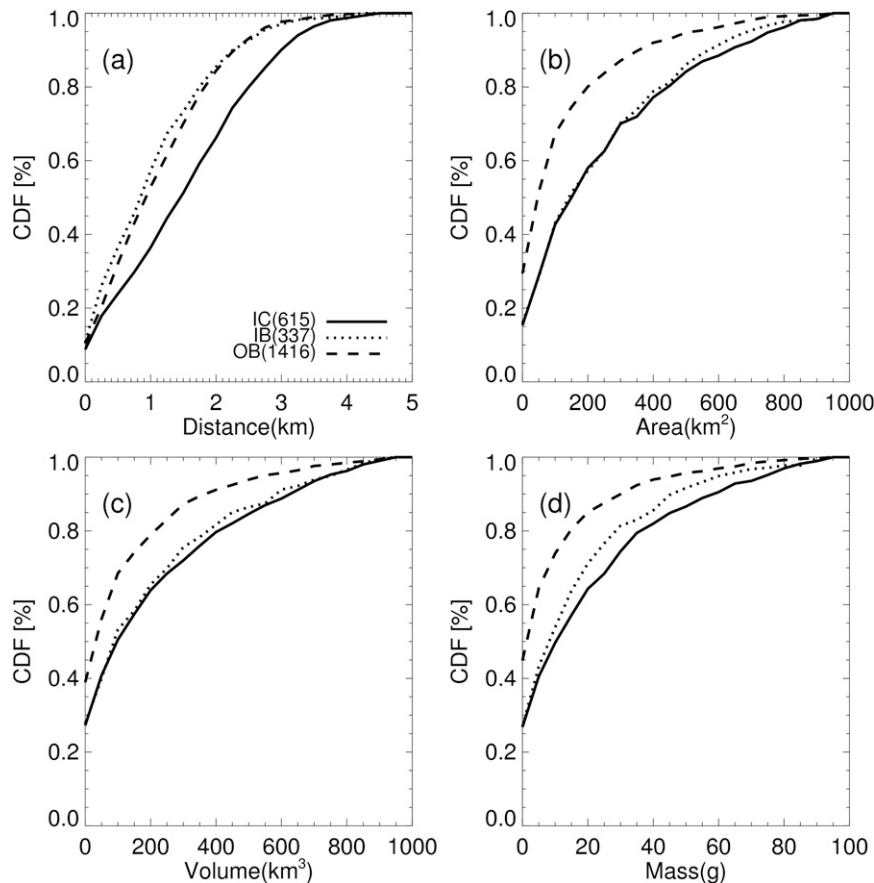
FIG. 7. CDFs of (a) overshooting distance, (b) overshooting area, (c) overshooting volume, and (d) overshooting precipitating ice mass for OTCPFs in the inner core (solid line), inner rainband (dotted line), and outer rainband (dashed line) regions.

Figure 7 presents the cumulative density functions of overshooting properties for OTCPFs in the IC, IB, and OB regions. From Fig. 7a, we can see that IC OTCPFs have the highest overshooting distance with a median value of 1.5 km. CDFs of overshooting distances in the IB and OB regions are very similar (with a median of about 0.9 km), and both are much lower than that in the IC region. About 56% of IC OTCPFs have overshooting distances greater than 1.5 km, while only 33% and 38% of those in the IB and OB regions, respectively, achieve that distance. As for the overshooting area (Fig. 7b), the distributions for IC and IB features are very similar while much lower values are found for OTCPFs in the OB region. For overshooting volume and ice mass (Figs. 7c,d), IC features produce the largest overshooting properties, followed by IB features. OB features produce the least overshooting volume and ice mass. Based on the significant test using analysis of variance, the differences among various TC regions for each overshooting parameter are statistically significant at the 99% level.

This is consistent with several previous studies. Cecil et al. (2002) studied the convective properties of 45 hurricanes observed by TRMM and indicated that convective precipitation is most often in the eyewall while stratiform precipitation is most readily found in the rainband regions. Using 10-yr TRMM data, Hence and Houze (2011) studied the vertical structure of hurricane eyewalls and indicated that the eyewall contains higher reflectivity and higher echo tops compared with rainband regions.

2) TC INTENSITY STAGES

To study the relationship between hot towers and TC intensity, the identified OTCPFs are classified into four TC intensity groups based on the Saffir–Simpson scale. They are tropical depression (TD), tropical storm (TS), category 1–2 hurricane (CAT1–2), and category 3–5 hurricane (CAT3–5) as shown in Table 4. The percentage of TCPFs that are hot towers is 1.83%, 1.66%, 1.20%, and 1.17%, respectively, for TD, TS, CAT 1–2, and CAT3–5. It is interesting to note that this percentage decreases as TC

TABLE 4. Populations of TCPFs and OTCPFs, and the percentage of OTCPFs associated with tropical depression (TD), tropical storm (TS), category 1–2 hurricanes (CAT1–2), and category 3–5 hurricanes (CAT3–5).

| Intensity	Maximum wind speed range (kt)	Population of OTCPFs	Population of TCPFs	Percentage of OTCPFs (%)
TD	$V_{max} < 34$	909	49 561	1.83
TS	$64 > V_{max} \geq 34$	922	55 544	1.66
CAT1–2	$64 \leq V_{max} \leq 95$	326	27 239	1.20
CAT3–5	$V_{max} > 95$	211	17 969	1.17

FIG. 8. The percentage of OTCPFs for different TC intensity stages in all TC regions and in the inner core, inner rainband, and outer rainband region only. For each group from left to right are percentage of OTCPFs for tropical depressions (TD), tropical storms (TS), category 1–2 hurricanes (CAT1–2), and category 3–5 hurricanes (CAT3–5), respectively.

intensity increases. However, for different TC regions, the results are very different. As shown in Fig. 8, in the IC region, the percentage of OTCPFs associated with hurricanes is higher (13% for CAT1–2 and 12% for CAT3–5) than that for TS (11%), which is higher than that for TD (7%). This indicates that as TC intensity increases, the percentage of IC features that are hot towers increases generally. However, when looking at IB, OB, and all TCPFs, the reverse is true (Fig. 8). A Pearson's chi-squared test has been done for Fig. 8 and the result indicates that statistically significant differences exist among different TC intensity stages in all TC regions, and in the IC, IB, and OB regions only at the 95% level.

CDFs of overshooting properties for identified OTCPFs associated with various TC intensity stages are presented in Fig. 9. From Fig. 9a, we can see that at lower frequencies (between 0% and 65% frequency), the greatest overshooting distance is found for OTCPFs related to TS, with lower values for TD and category 1–2 hurricane features, and the lowest for OTCPFs associated with category 3–5 hurricanes. The median values for TD, TS, CAT1–2, and CAT3–5 OTCPFs are 1.1, 1.2, 1.0, and 0.8 km, respectively. At higher frequencies (between 65% and 100%), the highest overshooting distance is found for OTCPFs associated with category 1–2 hurricanes, followed by TS, TD, and category 3–5 hurricanes features. The largest overshooting area is found for OTCPFs related to TS, with lower values for TD and category 1–2 hurricane features and the lowest for category 3–5 hurricane features (Fig. 9b). Similar results are also found for overshooting volume and precipitating ice mass (Figs. 9c,d). Overall, category 3–5 hurricane features are found to have the weakest overshooting properties. This may be because TCs reaching the strongest intensity stage have mostly fully developed and thus have less intense convection than weaker storms. According to the results from significance tests using analysis of variance, the differences among various TC intensity stages for each overshooting parameter are statistically significant at the 99% level.
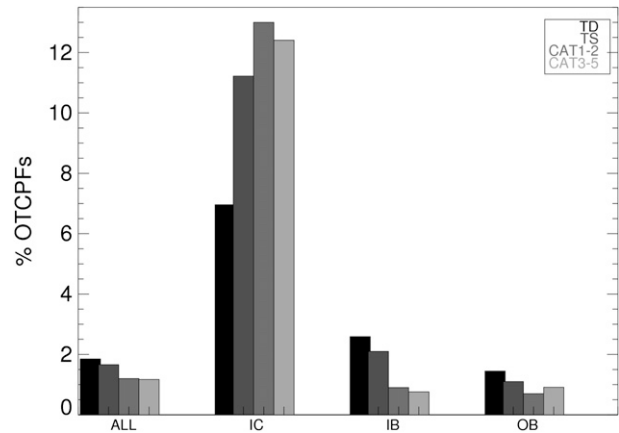
3) TC INTENSITY CHANGE STAGES

Jiang (2012) examined the probability of RI for TCs with or without hot towers in the inner core using TRMM data. Her statistics are based on each TRMM TC observation, that is, only the most convectively intense precipitation feature in the inner core is used. She found that the probability of RI is a factor of 2 higher for TCs with hot towers in the inner core than those without. In this study, our dataset contains all precipitation features not only in the inner core, but also in the inner rainband and outer rainband regions. Our goal here is to examine the percentage of TCPFs that are hot towers in different TC regions for different TC intensity change stages.

The "rapidly intensifying" threshold used in this study is 30 kt (15.4 m s^{-1}) (day)$^{-1}$ by following Kaplan and DeMaria (2003). As described in section 2a, here the 24-h future intensity change interpolated from the 6-hourly best-track data into TRMM overpass time is used to define intensity change categories. Three more intensity change categories—slowly intensifying (SI), neutral (N), and weakening (W)—are defined using equal-sized bins (Table 5). As a result, 248, 919, 996, and 205 OTCPFs are found associated with RI, SI, neutral, and weakening storms, respectively. The fraction of TCPFs that are hot towers in different TC regions for different TC intensity change stages is presented in Fig. 10. It can be seen that in all TC regions, TCPFs associated with RI have the highest percentage (2.04%) that overshoot 14 km, followed by SI (1.87%), N (1.49%), and W (0.93%). The percentage increases as the intensification rate increases. In the IC region, the trend is even more obvious. About 17% of IC
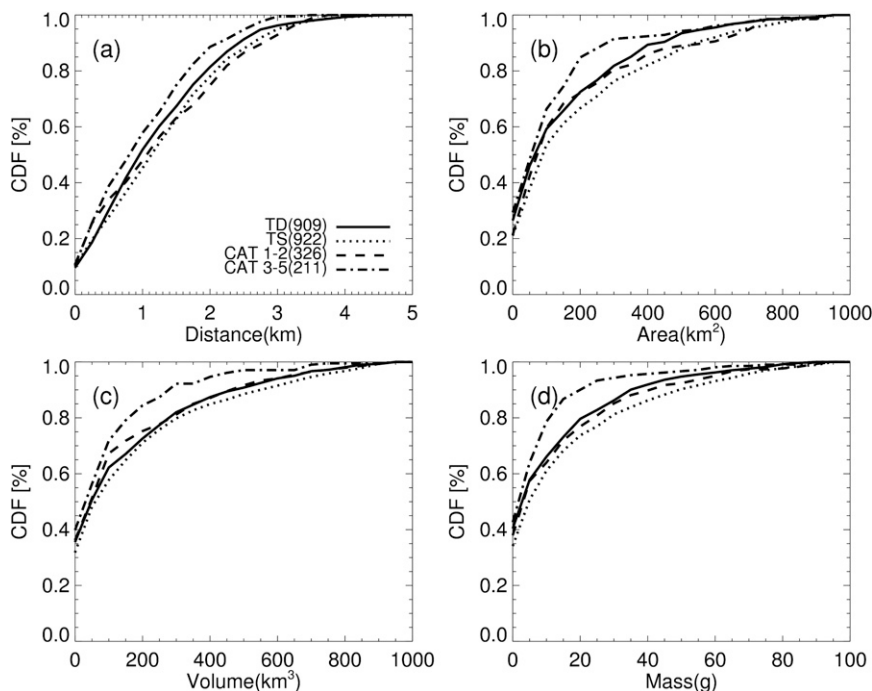
FIG. 9. CDFs of (a) overshooting distance, (b) overshooting area, (c) overshooting volume, and (d) overshooting precipitating ice mass for OTCPFs associated with tropical depressions (solid line), tropical storms (dotted line), category 1–2 hurricanes (dashed line), and category 3–5 hurricanes (dash–dotted line).

features in RI storms penetrate over 14 km, whereas the percentage is 11% for SI, 9% for neutral, and 8% for weakening storms. This suggests that a good correlation exists between the TC intensification rate and the percentage of features that are hot towers in the inner core region.

To determine the correlation quantitatively, the IC OTCPFs are first classified into several groups according to different TC intensification rate. Considering the sample size, here a bin of 10 kt per day is applied for each group. Then the fraction of OTCPFs for each TC intensification rate is calculated by dividing the number of OTCPFs by the number of TCPFs. To make the results more reliable, a threshold of at least 10 OTCPFs and 100 TCPFs is required for each qualified point. The result is shown in Fig. 11. It can be seen that as the fraction of

OTCPFs increases from 6.87% to 13.43%, the TC intensification rate increases from -25 to 35 kt $(day)^{-1}$. Furthermore, the linear regression reveals a very good linear relationship between TC intensification rate and the percentage of features that are hot towers in the IC region with a correlation coefficient of 0.94. Significance tests show that this correlation is statistically significant at the 99% level.

Back to Fig. 10, in the IB region, similar percentages of TCPFs that are hot towers are seen for RI and SI storms, with a smaller percentage for neutral storms and the smallest for weakening storms. However, in the OB region, although the percentage of OTCPFs is the highest for RI storms (3.5%), the second highest is for weakening storms (2.2%), followed by SI (1.4%) and neutral (1.0%) storms. Results from Pearson's chi-squared

TABLE 5. Populations of TCPFs and OTCPFs, and the percentage of OTCPFs associated with rapid intensification (RI), slow intensification (SI), neutral (N), and weakening (W) storms.

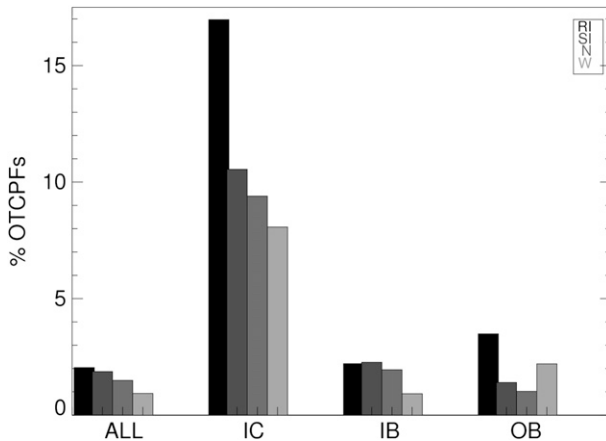| Intensity change	Maximum wind speed range (kt)	Population of OTCPFs	Population of TCPFs	Percentage of OTCPFs (%)
RI	$V_{max24} - V_{max} \geq 30$	248	12 147	2.04
SI	$30 > V_{max24} - V_{max} \geq 10$	919	49 176	1.87
N	$V_{max} - V_{max24} < 10, V_{max24} - V_{max} < 10$	996	66 994	1.49
W	$V_{max} - V_{max24} \geq 10$	205	21 996	0.93

FIG. 10. The percentage of OTCPFs for different TC intensity change stages in all TC regions and in the inner core, inner rainband, and outer rainband region only. For each group, from left to right are percentage of OTCPFs associated with rapid intensification (RI), slow intensification (SI), neutral (N), and weakening (W).
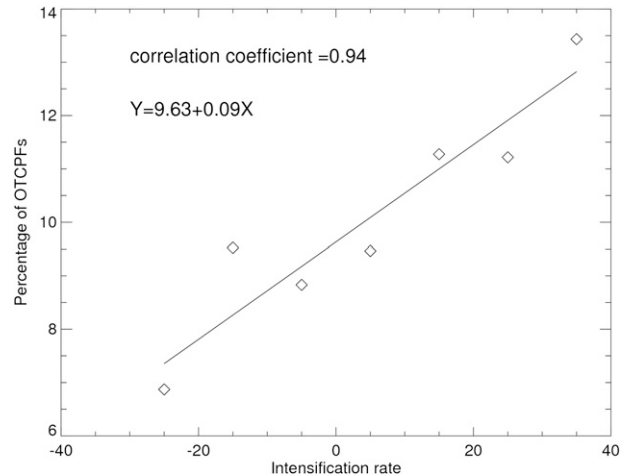

FIG. 11. Scatterplot of TC intensification rate vs percentage of OTCPFs in the inner core region. Correlation coefficient and the linear equation are shown at the top left.

tests for Fig. 10 show that statistically significant differences exist for the percentages of TCPFs that are hot towers among different TC intensity change stages in all TC regions, and in IC, IB, and OB regions only at the 95% level.

c. Convective properties of OTCPFs

To study the relationship between convective properties and overshooting properties of OTCPFs, four convective proxies—minimum 11-μm brightness temperature (T_{B11}) from the TRMM Visible and Infrared Scanner (VIRS), minimum 85- and 37-GHz polarization corrected temperature (PCT; Spencer et al. 1989) from the TRMM Microwave Imager (TMI), and maximum height of 40-dBZ radar echo from the TRMM PR—are selected to examine. The minimum T_{B11} here indicates how high a convective cloud can reach. The microwave brightness temperatures at 85 and 37 GHz respond to scattering of upwelling radiation by precipitation-sized ice particles, which reduce the observed brightness temperature. However, the low brightness temperature due to ice scattering could be confused with the sea surface, which also appears cold due to low sea surface emissivity in 85- and 37-GHz channels. The PCT at 85 GHz (Spencer et al. 1989) and 37 GHz (Cecil et al. 2002) is defined to remove the ambiguity in such a way that PCTs are cold for ice scattering and warm for the sea surface regions. The minimum 85- and 37-GHz PCT depend on the optical path of frozen hydrometeors. The 85-GHz channel responds to smaller ice particles, while the 37-GHz channel is influenced more by larger particles.

The correlation coefficient is calculated between four overshooting properties and four convective parameters (Table 6). Generally, a moderate correlation exists between overshooting properties and convective parameters, with correlation coefficients ranging from 0.33 to 0.61, all of which are statistically significant at 99% level. The convective intensity increases as the overshooting distance, area, volume, and ice mass increase. For overshooting distance, the highest correlation coefficient is found with minimum T_{B11}, with a correlation coefficient of −0.61. Since T_{B11} indicates the cold cloud-top height, it is expected that this parameter is well correlated with the overshooting distance. The overshooting area, volume, and precipitating ice mass correlate the best with minimum 37-GHz PCT with correlation coefficients of −0.59, −0.59, and −0.60, respectively. This suggests that OTCPFs with larger overshooting area, volume, and ice mass tend to have greater ice water path contributed by larger ice particles.

4. Conclusions

Using the 11-yr TRMM TCPF database, TCPFs that are hot towers (OTCPFs) are identified based on five reference levels. It is found that only 1.59% of deep convective systems in TCs have 20-dBZ radar echoes reaching 14 km and only 0.09% of them even reach the 380-K potential temperature level. Given the geographical distribution of OTCPFs show little sensitivity to various reference heights; considering the smaller sample sizes when using higher reference levels, 14 km is chosen to identify hot towers in the rest of the study. Emphasis is placed on the geographical and seasonal variations of hot towers in TCs

TABLE 6. The correlation coefficients between each overshooting property (including overshooting distance, area, volume, and ice mass) and convective parameter [including minimum 11-μm brightness temperature (Min T_{B11}), minimum 85- and 37-GHz polarization corrected temperature (Min PCT_{85} and Min PCT_{37}), and the maximum heights of PR 40 dBZ (Max Z_{40dBZ})] for identified OTCPFs.

Coefficient correlations	Min T_{B11}	Min PCT_{85}	Min PCT_{37}	Max Z_{40dBZ}
Distance	−0.61	−0.55	−0.52	0.46
Area	−0.38	−0.52	−0.59	0.33
Volume	−0.40	−0.51	−0.59	0.35
Ice mass	−0.44	−0.52	−0.60	0.36

and how hot towers are distributed in different TC regions and intensity and intensity change stages.

Among six TC-prone oceanic basins, the highest population of TC convective systems (TCPFs) and TCPFs that are hot towers (OTCPFs) is found over the northwest Pacific basin. However, the greatest percentage of TCPFs that are hot towers is found over the North Indian Ocean basin. OTCPFs in this basin also have larger overshooting distance and ice mass, although it has the lowest population of both TCPFs and OTCPFs. The analysis of seasonal variations shows that both the population and overshooting properties of OTCPFs is driven by the monthly activities of TCs.

For different TC regions, it is found that TCPFs in the IC region have the highest chance (11%) to overshoot above 14 km, while the percentage of OTCPFs is only 2% and 1% in the IB and OB regions, respectively. OTCPFs in the IC region have much larger overshooting distance, area, volume, and ice mass than those in the IB and OB regions. It is also shown that the highest fraction of OTCPFs found in the NIO basin is mostly contributed by OTCPFs in the OB region. In the IC and IB region, higher percentages of TCPFs with hot towers are in the SPA and NWP basins.

In the IC region only, the percentage of TCPFs that are hot towers increases as TC intensity increases. However, when looking at IB, OB, and all TCPFs, the reverse is true. It is also interesting to note that the smallest overshooting distance, area, volume, and ice mass are found for OTCPFs in category 3–5 hurricanes. This may be because TCs reaching the strongest intensity stage have mostly fully developed thus have less intense convection than weaker storms.

For different TC intensity change categories, it is found that the percentage of TCPFs that are hot towers increases as the intensification rate increases, especially in the inner core region. About 17% of IC features in

RI storms penetrate over 14 km, while the percentage is down to 11% for SI, 9% for neutral, and 8% for weakening storms. A linear regression has been applied to determine the correlation between the TC intensification rate and the percentage of TCPFs that are hot towers in the IC region quantitatively. The result shows a very good linear relationship between these two parameters with a correlation coefficient of 0.94.

The relationship between convective properties and overshooting properties of OTCPFs are examined. The overshooting distance correlates best with minimum 11-μm brightness temperature. For overshooting area, volume, and ice mass, the best correlations are found with minimum 37-GHz PCT. This suggests that OTCPFs with larger overshooting area, volume and ice mass tend to produce larger ice particles.

APPENDIX

List of Acronyms and Abbreviations

ATL	Atlantic
CAPE	Convective available potential energy
CAT1–2	Category 1–2 hurricanes
CAT3–5	Category 3–5 hurricanes
CDFs	Cumulative distribution functions
EPA	East central Pacific
IB	Inner rainband
IC	Inner core
LNB	Level of neutral buoyancy
LNB_{sfc}	Level of neutral buoyancy calculated using NCEP sounding and surface equivalent potential temperature

$LNB_{925\&1000}$	Level of neutral buoyancy calculated using potential temperature at 925 and 1000 mb
N	Neutral
NIO	North Indian Ocean
NWP	Northwest Pacific
OB	Outer rainband
OTCPF	Overshooting tropical cyclone precipitation features
PCT	Polarization corrected temperature
PR	Precipitation radar
PFs	Precipitation features
RI	Rapid intensification
SI	Slow intensification
SIO	South Indian Ocean
SPA	South Pacific
T_{B11}	Minimum 11-μm brightness temperature
TC	Tropical cyclone
TCPF	Tropical cyclone precipitation features
TD	Tropical depression
TMI	Tropical Rainfall Measuring Mission Microwave Imager
TRMM	Tropical Rainfall Measuring Mission
TS	Tropical storm
VIRS	Visible and Infrared Scanner
W	Weakening
Z_{trop}	Level of NCEP reanalysis tropopause
Z_{380K}	Level of 380-K potential temperature

REFERENCES

Adler, R. F., G. J. Huffman, D. T. Bolvin, S. Curtis, and E. J. Nelkin, 2000: Tropical rainfall distributions determined using TRMM combined with other satellite and rain gauge information. *J. Appl. Meteor.,* **39,** 2007–2023.

Cecil, D. J., E. J. Zipser, and S. W. Nesbitt, 2002: Reflectivity, ice scattering, and lightning characteristics of hurricane eyewalls and rainbands. Part I: Quantitative description. *Mon. Wea. Rev.,* **130,** 769–784.

——, S. J. Goodman, D. J. Boccippio, E. J. Zipser, and S. W. Nesbitt, 2005: Three years of TRMM precipitation features. Part I: Radar, radiometric, and lightning characteristics. *Mon. Wea. Rev.,* **133,** 543–566.

Dessler, A. E., 2002: The effect of deep, tropical convection on the tropical tropopause layer. *J. Geophys. Res.,* **107,** 4033, doi:10.1029/2001JD000511.

Gettelman, A., M. L. Salby, and F. Sassi, 2002: The distribution and influence of convection in the tropical tropopause region. *J. Geophys. Res.,* **107,** 4080, doi:10.1029/2001JD001048.

Gray, W. M., 1968: Global view of the origin of tropical disturbances and storms. *Mon. Wea. Rev.,* **96,** 669–700.

Hall, T. J., and T. H. Vonder Haar, 1999: The diurnal cycle of west Pacific deep convection and its relation to the spatial and temporal variations of tropical MCSs. *J. Atmos. Sci.,* **56,** 3401–3415.

Hence, D. A., and R. A. Houze, 2011: Vertical structure of hurricane eyewalls as seen by the TRMM Precipitation Radar. *J. Atmos. Sci.,* **68,** 1637–1652.

Hendricks, E. A., M. T. Montgomery, and C. A. Davis, 2004: The role of "vortical" hot towers in the formation of Tropical Cyclone Diana (1984). *J. Atmos. Sci.,* **61,** 1209–1232.

Holton, J. R., P. H. Haynes, M. E. McIntyre, A. R. Douglass, R. B. Rood, and L. Pfister, 1995: Stratosphere–troposphere exchange. *Rev. Geophys.,* **33,** 403–439.

Houze, R. A., Jr., W. Lee, and M. M. Bell, 2009: Convective contribution to the genesis of Hurricane Ophelia (2005). *Mon. Wea. Rev.,* **137,** 2778–2800.

Iguchi, T., T. Kozu, R. Meneghini, J. Awaka, and K. Okamoto, 2000: Rain-profiling algorithm for the TRMM Precipitation Radar. *J. Appl. Meteor.,* **39,** 2038–2052.

Jiang, H., 2012: The relationship between tropical cyclone intensity change and the strength of inner-core convection. *Mon. Wea. Rew.,* **140,** 1164–1176.

——, and E. J. Zipser, 2010: Contribution of tropical cyclones to the global precipitation from eight seasons of TRMM data: Regional, seasonal, and interannual variations. *J. Climate,* **23,** 1526–1543.

——, C. Liu, and E. J. Zipser, 2011: A TRMM-based tropical cyclone cloud and precipitation feature database. *J. Appl. Meteor. Climatol.,* **50,** 1255–1274.

——, E. M. Ramirez, and D. J. Cecil, 2013: Convective and rainfall properties of tropical cyclone inner cores and rainbands from 11 years of TRMM data. *Mon. Wea. Rew.,* **141,** 431–450.

Jiang, J. H., B. Wang, K. Goya, K. Hocke, S. F. Eckermann, J. Ma, D. L. Wu, and W. G. Read, 2004: Geographical distribution and interseasonal variability of tropical deep convection: UARS MLS observations and analyses. *J. Geophys. Res.,* **109,** D03111, doi:10.1029/2003JD003756.

Kaplan, J., and M. DeMaria, 2003: Large-scale characteristics of rapidly intensifying tropical cyclones in the North Atlantic basin. *Wea. Forecasting,* **18,** 1093–1108.

Kelley, O. A., J. Stout, and J. B. Halverson, 2004: Tall precipitation cells in tropical cyclone eyewalls are associated with tropical cyclone intensification. *Geophys. Res. Lett.,* **31,** L24112, doi:10.1029/2004GL021616.

——, ——, and ——, 2005: Hurricane intensification detected by continuously monitoring tall precipitation in the eyewall. *Geophys. Res. Lett.,* **32,** L20819, doi:10.1029/2005GL023583.

Kistler, R., and Coauthors, 2001: The NCEP–NCAR 50-Year Reanalysis: Monthly means CD-ROM and documentation. *Bull. Amer. Meteor. Soc.,* **82,** 247–267.

Liu, C., and E. J. Zipser, 2005: Global distribution of convection penetrating the tropical tropopause. *J. Geophys. Res.,* **110,** D23104, doi:10.1029/2005JD006063.

——, ——, and S. W. Nesbitt, 2007: Global distribution of tropical deep convection: Different perspectives form TRMM infrared and radar data. *J. Climate,* **20,** 489–503.

——, ——, D. J. Cecil, S. W. Nesbitt, and S. Sherwood, 2008: A cloud and precipitation feature database from 9 years of TRMM observations. *J. Appl. Meteor. Climatol.,* **47,** 2712–2728.

Montgomery, M. T., M. E. Nicholls, T. A. Cram, and A. B. Saunders, 2006: A vortical hot tower route to tropical cyclogenesis. *J. Atmos. Sci.,* **63,** 355–386.

Nesbitt, S. W., E. J. Zipser, and D. J. Cecil, 2000: A census of precipitation features in the tropics using TRMM: Radar, ice scattering, and lightning observations. *J. Climate,* **13,** 4087–4106.

Petersen, W. A., and S. A. Rutledge, 2001: Regional variability in tropical convection: Observations from TRMM. *J. Climate,* **14,** 3566–3586.

Riehl, H., and J. S. Malkus, 1958: On the heat balance in the equatorial trough zone. *Geophysica,* **6,** 503–538.

Romps, D. M., and Z. M. Kuang, 2009: Overshooting convection in tropical cyclones. *Geophys. Res. Lett.,* **36,** L09804, doi:10.1029/2009GL037396.

Rosenlof, K. H., 1995: The seasonal cycle of the residual mean meridional circulation in the stratosphere. *J. Geophys. Res.,* **100** (D3), 5173–5191.

Schumacher, C., and R. A. Houze Jr., 2003: Stratiform rain in the tropics as seen by the TRMM Precipitation Radar. *J. Climate,* **16,** 1739–1756.

Simpson, J., 1990: Global circulation and tropical cloud activity. *Proc. Int. Symp. on Aqua and Planet,* Tokyo, Japan, Tokai University, 77–90.

Spencer, R. W., H. M. Goodman, and R. E. Hood, 1989: Precipitation retrieval over land and ocean with the SSM/I: Identification and characteristics of the scattering signal. *J. Atmos. Oceanic Technol.,* **6,** 254–273.

Yulaeva, E., J. R. Holton, and J. M. Wallace, 1994: On the cause of the annual cycle in the tropical lower-stratospheric temperatures. *J. Atmos. Sci.,* **51,** 169–174.

Zipser, E. J., D. Cecil, C. Liu, S. Nesbitt, and D. Yorty, 2006: Where are the most intense thunderstorms on earth? *Bull. Amer. Meteor. Soc.,* **87,** 1057–1071.